Pergamon

Acta Materialia 50 (2002) 2639–2654

Acta MATERIALIA

www.actamat-journals.com

The oxidation behaviour of an AZ91D magnesium alloy at high temperatures

F. Czerwinski *

Thixosystems, Husky Injection Molding Systems Ltd., Bolton, Ontario, L7E 5S5 Canada

Received 5 February 2001; received in revised form 26 February 2002; accepted 3 March 2002

Abstract

As-cast AZ91D magnesium alloy was exposed to air in the temperature range from 470 to 800 K for time intervals up to 10 h. Thermogravimetric measurements revealed three distinct stages of the reaction where an initial formation of protective oxide was followed by an incubation period with a subsequent transient to non-protective oxidation, at a rate either constant or sharply increasing over time. The approximate temperature and time frames for an onset of each stage were identified. A strong link was found between the oxidation kinetics and the scale morphology. The initial protective film, grown anisotropically over the microstructural features of the substrate, was transformed to oxide ridges. The non-protective oxidation was associated with a formation of oxide nodules and their further coalescence into a fine-grained scale of a loose structure. All the morphologies were comprised of a randomly oriented magnesium oxide MgO with traces of $MgAl_2O_4$ spinel. The oxidation mechanism represented a complex reaction where morphological and phase transformations within the alloy substrate were accompanied by magnesium sublimation/evaporation and subsequent condensation within the scale pores or cracks, and superimposed on the reaction with oxygen. Some implications for the high temperature processing of magnesium alloys are discussed.

Keywords: Magnesium alloys; Oxidation; thixomolding

1. Introduction

Magnesium alloys, during typical applications, are subjected to environmental conditions ranging from indoor atmospheres, for household or electronic appliances, to intermittent salt splashes for some automotive components. As a result, a majority of studies devoted to oxide growth on magnesium alloys describes room temperature phenomena and liquid environments [1,2]. It has been agreed that the initial reaction of pure magnesium with oxygen proceeds in three stages: oxygen chemisorption below the topmost magnesium layer, formation and coalescence of oxide islands and oxide thickening [3]. Contact with water vapour leads also to an oxide growth, but the rate of reaction is much slower and the oxide layer contains relatively large amounts of hydroxyl or hydroxide species [4,5].

There are, however, manufacturing stages when

* Fax: +1-905-951-5365.
E-mail address: fczerwinski@husky.ca (F. Czerwinski).

1359-6454/02/$22.00
PII: S1359-6454(02)00094-0

magnesium alloys are exposed to high temperatures and detrimental contact with an oxidizing medium. This refers to heat treatment, welding, casting and in particular to the novel route of semisolid processing called thixomolding® [6,7]. An extremely high affinity of magnesium to oxygen along with the highly developed surface area of Mg alloy chips, used as a feedstock during thixomolding®, make the system prone to oxidation. It is anticipated that alloy protection inside the thixomachine barrel by an inert atmosphere of argon, is essentially better than molten surface shielding by SF_6 gas during die casting [8]. So far there is a lack of experimental verification and existing data provide a rather unclear message. Firstly, the inertness of an Ar atmosphere is sensitive to small amounts of entrapped air and the growth rate of MgO on Al-based alloy at temperatures of 723–1073 K in a mixture of Ar+1%O_2 and Ar+5%O_2 equals to 25% and 70%, respectively, of the oxidation rate in air [9]. Secondly, the final oxygen content in thixomolded parts is still about one order of magnitude higher than that present in an initial feedstock [8]. A description of the alloy oxidation behaviour is therefore of key importance for designing material feeding and Ar flow systems. It is also important for feedstock manufacturing in terms of morphology and its chemical modification against oxidation. In particular, it will help to verify the necessity of beryllium additions routinely used in conventionally cast alloys.

In order to identify factors controlling surface degradation at high temperatures, a research was conducted which involved commercial Mg–Al–Zn alloys in solid and semisolid states, exposed to various atmospheres simulating thixo-processing. This study describes thermogravimetric kinetics, microstructural characteristics and the reaction mechanism following exposure to air.

2. Experimental details

The material used for oxidation tests was a commercial AZ91D magnesium alloy, manufactured by Solikamsk Desulfurized Works (Russia). According to chemical analysis, conducted using an Inductively Coupled Argon Plasma Mass Spectrometer and following ASTM E1097-97 (modified) and E1479-99 standards, the alloy contained 8.94% Al, 0.59% Zn, 0.34% Mn, 0.0005% Ni, 0.002% Fe, less than 0.005% Si, less than 0.001% Cu, less than 0.005% each of Zr, Sn, Pb and Mg balance. The Be content, being of particular interest in this test, was at a level of 5±0.15 ppm as remaining from the primary metallurgical process. Specimens, in the form of 8×6×1.5 mm coupons, were sectioned from the central part of the as-cast ingot and mechanically polished with a 2400 silicon carbide paper as the final stage. To minimize the amount of the oxide formed during room temperature exposure, the samples were installed in the thermogravimetric analyzer (TGA) directly after polishing and degreasing in ethanol. The Perkin Elmer TGA7 apparatus was capable of accommodating a specimen with the maximum weight of 0.5 g and had a measurement accuracy of 1 μg. The reaction temperature was monitored by a Pt/Pt–Rh thermocouple mounted within a furnace at a distance of 2 mm from the specimen surface. Weight change kinetics were measured in air under isothermal conditions at temperatures between 470 and 760 K. The specimens were inserted into a chamber at room temperature and heated to the reaction temperature at a rate of 100 K/min. Although the major effort was focused on time intervals shorter than 1 h, for certain conditions the measurements were extended up to 10 h. To prevent the ignition of the magnesium alloy within the TGA apparatus, the oxidation experiments at temperatures higher than 760 K were performed within a tube furnace with enhanced safety features. In addition to macroscopical observations, the alloy surface, after high-temperature exposure, was investigated by scanning electron microscopy (SEM) equipped with an energy dispersive X-ray analyzer (EDAX). Phase identification was conducted using an X-ray diffractometer and $Cu_{K\alpha}$ radiation. The microstructure of the magnesium alloy substrate, before and after high temperature exposures, was examined on polished cross-sections after etching with 2% nital.

3. Results

3.1. Thermogravimetric analysis

Results of thermogravimetric measurements revealed the complex character of alloy weight change versus time. As seen in Fig. 1(a), the very initial stage of air exposure at temperatures in the range of 470–800 K was characterized by rapid weight gain, similar for all samples. However, after a time interval of 2–4 min and a corresponding weight gain of 20–25 μg/cm^2, the further reaction kinetics depended on the temperature. While samples tested at 745 K and 760 K continued to increase their weight at a significantly lower rate, the samples subjected to temperatures lower than 670 K experienced a weight reduction. In general, the lower the test temperature, the faster and larger weight loss of the sample was observed.

The effect of test temperature on weight change curves was also evident during the transient stage. The transient stage is understood here as the time before an onset of accelerated oxidation and some exemplary curves for a maximum time interval of 1 h are shown in Fig. 1(b). The alloy tested at a temperature of 470 K did not change its weight for up to 1 h. At the same time, the measurement conducted for the same alloy tested at 710 K revealed an accelerated weight gain after approximately 30 min of the reaction. An increase of the temperature up to 745 K essentially changed the thermogravimetric curves, which showed a rapid rise after the transient stage. The time of rapid weight gain was approximately 20 and 15 min for reaction temperatures of 745 K and 760 K, respectively. Since the magnesium alloy exposed to air at temperatures higher than 710 K exhibited a catastrophic oxidation relatively fast, it was only possible to conduct the long-term thermogravimetric tests at lower temperatures. The weight change curves recorded below 710 K and time intervals up to 10 h are plotted in Fig. 1(c). It is clear that at temperatures of 570 K and 610 K the sample weight remained practically constant over the whole range of time intervals examined here. A slight but continuous weight increase was observed for the alloy tested at 660 K. Such characteristics indicate so-called linear oxidation at a constant rate. The curve for the alloy exposed at 740 K, which experienced a rapid weight gain, is shown for comparison in the left-hand part of the plot in Fig. 1(c).

3.2. Macroscopic observations

A simple visual assessment indicates that the morphology of the oxide growth surfaces depended both on the temperature and time of the reaction. Some typical examples are shown in Fig. 2. At a temperature of 675 K, no significant differences were macroscopically detected for exposure times as long as 12 h (Fig. 2(a)). A change of the surface color from bright metallic to matt gray suggests the formation of a macroscopically uniform layer of oxide and this was essentially true for all temperatures below 710 K. By increasing the temperature over 710 K, the exposure time exerted a primary influence. There was initially an incubatory period of time after which the macroscopically uniform oxidation front was not stable and nodular growth was activated. An example of the morphology formed after 1 h at 745 K is shown in Fig. 2(b) where numerous dark oxide nodules extend above the specimen surface. At temperatures higher than 745 K, nodular growth was the dominant oxidation mechanism and after 1 h exposure at 770 K, nodules coalesced into a continuous layer which almost covered the entire alloy surface (Fig. 2(c)).

A further increase in the air temperature above 780 K made the alloy prone to ignition. At 840 K the incubation time preceding ignition lasted between 10 and 15 min. Usually, the ignition took place simultaneously in several spots and spread over the entire sample surface of approximately 200 mm^2. On a macroscopical scale the material exhibited inhomogeneity in terms of both the color and morphology, suggesting nonuniformity in a distribution of combustion heat, generated over the reaction area. As seen in Fig. 2(d), it is still possible to distinguish the oxide formed before ignition as well as the products of direct metal combustion.

3.3. Microscopic examination of oxides and substrates

3.3.1. Cross-sectional observations

An analysis of polished cross-sections aimed to reveal the internal structure of the oxide, the inter-

(a)

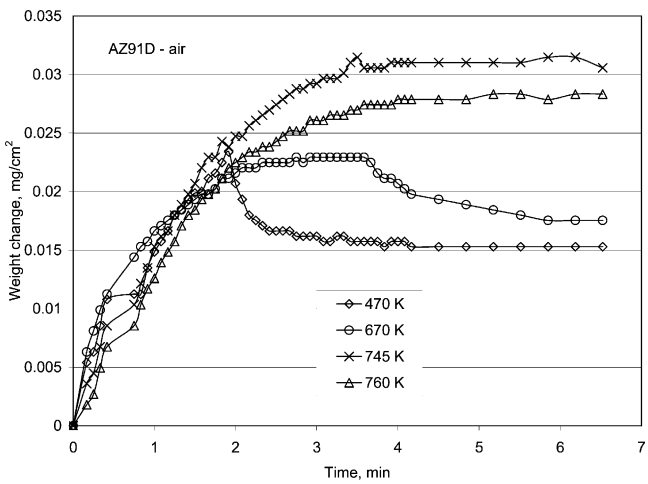
AZ91D - air
Weight change, mg/cm2
Time, min
470 K
670 K
745 K
760 K

(b)

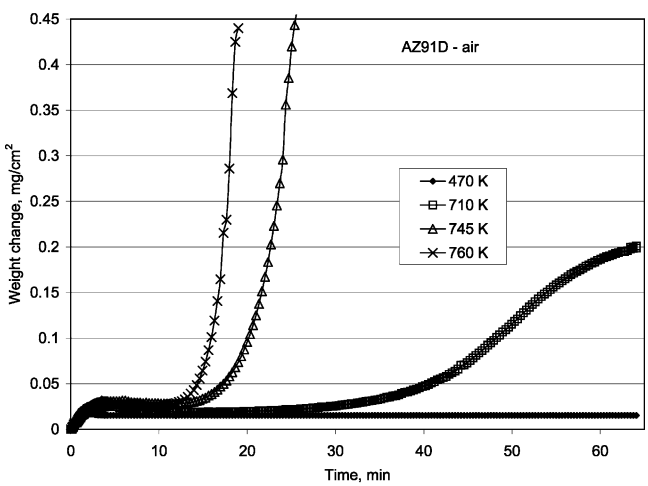
AZ91D - air
Weight change, mg/cm2
Time, min
470 K
710 K
745 K
760 K

(c)

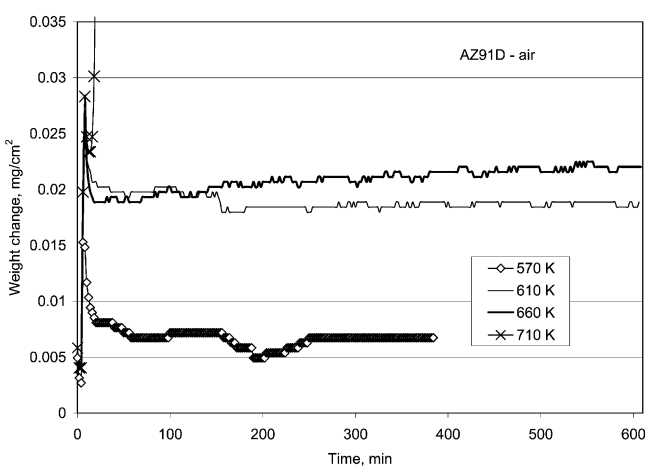
AZ91D - air
Weight change, mg/cm2
Time, min
570 K
610 K
660 K
710 K

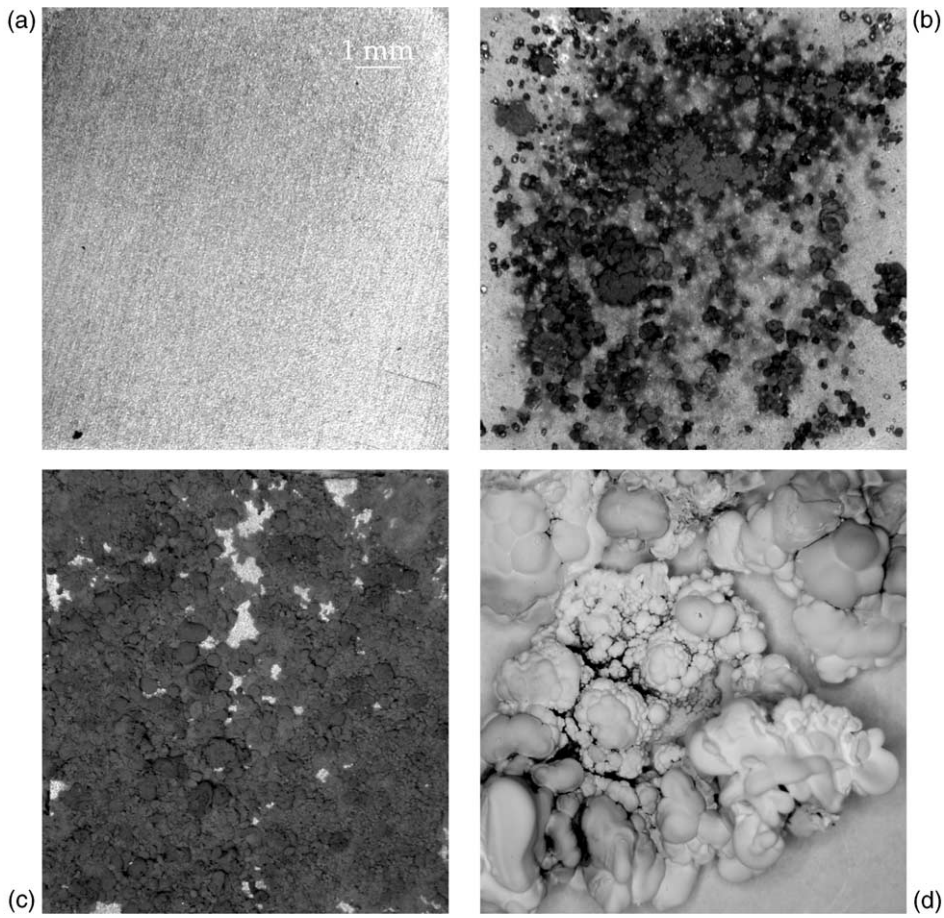

Fig. 2. Macroscopic images of AZ91D alloy surfaces after air exposures: (a) 660 K, 10 h; (b) 745 K, 1 h ; (c) 770 K, 1 h; (d) 820 K, 10 min.

face between the oxide and metal, as well as the metallic substrate itself. As-cast alloy consisted of dendritic grains with two phases of α-Mg and intermetallics. Morphologically, the massive intermetallics, the eutectics as a lamellar structure of intermetallics and α-Mg, or a mixture of both components, were distributed along the α-Mg grain boundaries (Fig. 3(a)). The image contrast shows that there were also some minor phases with the morphologies suggesting Al–Fe–Mn intermetallics and Mg_2Si inclusions, originated from a metallurgical rectification of the alloy. It should be noted that precipitates of minor phases, particularly that believed to be Mg_2Si easily developed oxide films during sample preparation, as indicated by the arrows in Fig. 3(a). The oxide films formed at temperatures lower than approximately 710 K were too thin for cross-sectional imaging with the optical microscopy and the main effect of the heat was expressed by microstructure changes within the substrate, especially clear after long-term exposures. Since, at the reaction temperature, all

Fig. 1. Thermogravimetric measurements of weight change versus time for an as-cast AZ91D alloy in an air environment: (a) initial stage reaction at temperatures between 470 and 760 K; (b) exemplary kinetics for a maximum time interval of 1 h showing the incubation period and non-protective oxidation; (c) long term exposure curves at temperatures between 570 and 710 K.

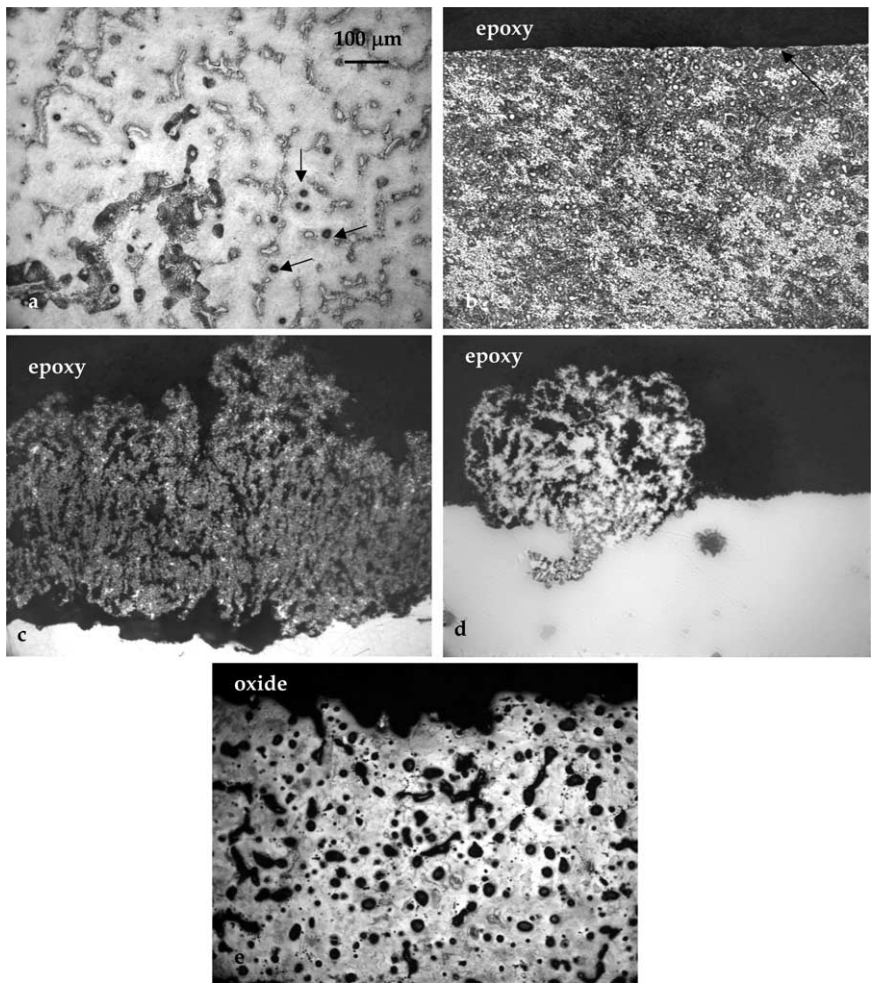

Fig. 3. Cross-sectional images of an AZ91D alloy and oxides grown after air exposure: (a) as cast alloy with arrows indicating precipitates covered with an oxide during polishing; (b) spheroidal precipitates in the alloy oxidized for 16 h at 693 K; the arrow points out the oxidized surface; (c) oxide grown after 20 min at 768 K, sample without etching; (d) individual nodule formed after 5 min at 800 K, sample without etching; (e) oxide formed after 17 min at 800 K. Unless specified—etched with a nital. The epoxy used for the sample mounting is indicated.

the alloy components were in solid state, the major change is a spheroidization of the intermetallic phase and its gradual dissolution within the matrix (Fig. 3(b)).

The cross-section of nodules revealed that they were composed of dark oxide and white inclusions representing a metal (Fig. 3(c)). While metal particles of the order of micrometers were densely distributed within the oxide, large voids were present at the substrate–nodule interface. Besides this, there were numerous channels oriented from the substrate towards the gas/oxide interface. Increasing the temperature to 800 K influenced the nodule microstructure and the most noticeable change was the higher contribution of the metallic phase (Fig. 3(d)). Although the oxide/metal interface contains voids similar to that developed at 768 K, the novel feature is the selective oxidation of the substrate with the oxide penetrating deep into the substrate material. The higher the temperature, the deeper the penetration of the oxide into the substrate. After long-term exposures at 800 K, the oxide for-

med a continuous layer with essentially the same microstructure as characterized above for individual nodules. Since, in order to reveal the substrate microstructure, the sample was subjected to etching, the small metallic particles within the scale disappeared (Fig. 3(e)). At 800 K the alloy was in a semi-solid state and the dark spherical shaped features correspond to the islands being liquid at the reaction temperature. As a result of selective oxidation the oxide/metal interface is serrated showing numerous protrusions.

3.3.2. Analysis of oxide growth surfaces

Observations of the planar alloy surface subjected to high temperatures allowed us to register the oxide growth under magnifications of optical microscopy. At the beginning, the oxide thickness did not depend clearly on the crystallographic orientation of the substrate grains. The first oxide nuclei were formed on some specific microstructural features of the substrate well before it was possible to detect the continuous layer. The preferential sites for oxide growth were the intersections of some grain boundaries with the alloy surface. However, the most important features causing oxidation anisotropy was the alloy phase composition (Fig. 4(a)). While at 706 K areas surrounding intermetallic phase acted as sites for accelerated oxidation, at 790 K the intermetallic phase itself was fast transformed into the oxide (Fig. 4(b)).

SEM examinations revealed that the macroscopically flat and smooth oxide scale formed during the transient period is, in fact, relatively rough covered with nonuniform growth features (Fig. 4(a)). The protrusions, called “ridges”, grow usually in the through-scale cracks. Although it is difficult to conclude oxide grain size from the surface morphology, the estimated oxide grain is around 5–10 μm (Fig. 4(d)). The oxide nodules imaged under the magnification of SEM revealed their highly irregular shape (Fig. 5(a)). Each nodule contained numerous craters connecting the surface with the substrate alloy (Fig. 5(b)). The fresh oxide formed around craters was very fine grained and had an appearance of a relatively loose, powder-like material (Fig. 5(c)). The macroscopically flat area surrounding nodules also contained microscopic growth features. As seen in Fig. 5(d), the surface is covered with numerous small pits and patches of fresh oxide with a matrix exhibiting a quite compact structure. Since, according to the principle of image formation in SEM, bright areas indicate the gathering of electrons, the bright component should have a lower electrical conductivity, suggesting the possibility of a difference in phase composition. The bright component forms ridges on the top of the nodules (Fig. 5(a)) as well as some irregular precipitates on flat areas (Fig. 5(d)).

In addition to small metal particles inside the nodule discussed above, SEM revealed a thin metallic layer on the nodule/gas interface (Fig. 6(a)). The microchemical segregation over the oxide surface was examined using the SEM/EDAX technique with a focus on the difference in chemical composition between the nodule and the surrounding area. Exemplary spectra are shown in Fig. 6(b) and (c). A comparison of Al and Mg peak intensities from energy spectra revealed that the nodule area contained significantly more Al than the surrounding area. A low intensity of Zn peak formed by its 0.59% addition makes it difficult to assess differences and at least, for a first approximation, the concentrations are similar. Manganese added in the quantity of 0.34% to transform the iron and other heavy-metal elements into relatively harmless intermetallic compounds is in the area surrounding the nodules.

3.4. X-ray diffraction measurement of phase composition

Several typical systems were selected for X-ray examination including a bare substrate, the substrate covered with thin oxide grown during early-stage reaction, a product of total oxidation of the metallic substrate and a product of combustion of a partly oxidized alloy. Air exposure at 750 K for 5 min produced a uniform oxide with the morphology discussed previously. Surprisingly, X-ray diffraction analysis did not detect a crystallographic phase on the alloy surface (Fig. 7(a)). The diffraction pattern contains a majority of peaks characteristic for Mg and three peaks which can be ascribed to the $Mg_{17}Al_{12}$ phase. It should be noted that the location of the strongest peak for $Mg_{17}Al_{12}$

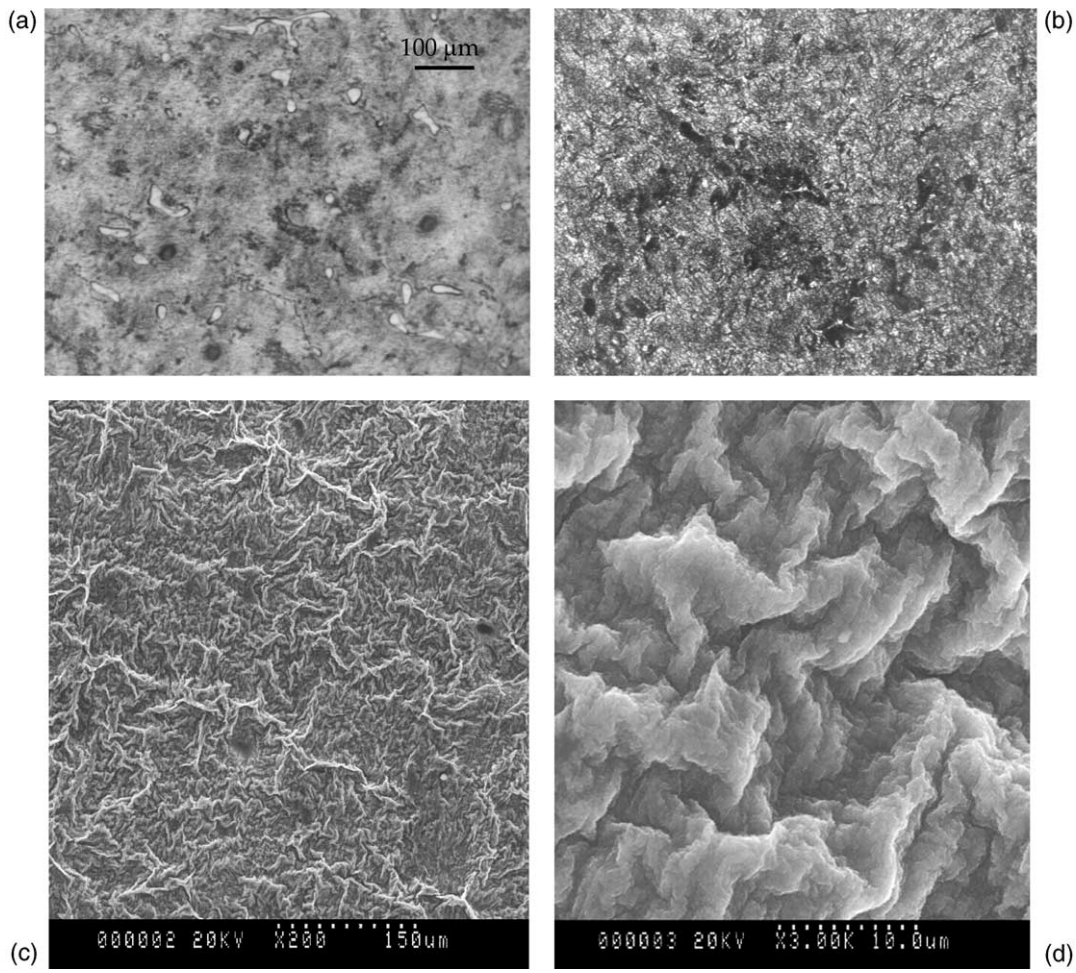

Fig. 4. Top-view morphology of the oxide formed on an AZ91D during the early stage reaction: (a) 706 K, 10 min, intermetallics seen as a white phase; (b) 790 K, 5 min, areas covered by the intermetallics seen as dark, optical microscopy; (c) 760 K, 1 min general view of oxide surface, SEM; (d) magnified part of the area between ridges of (c), SEM.

at 2-theta of 36.191 deg is very close to the strongest peak of the $MgAl_2O_4$ spinel at 2-theta of 36.853 deg. In order to exclude the possible spinel contribution, the oxide was removed by mechanical polishing using sandpaper and the substrate was subjected to X-ray re-examination. Results shown in Fig. 7(b) indicate that intensities of Mg peaks increased by one order of magnitude after the removal of the oxide absorbing the X-ray radiation. Some change in relative intensities of Mg peaks might be caused by the crystallographic texture introduced by the surface deformation. A diffraction peak at 2-theta of 36 deg is still present, though its intensity is low. A comparison of both spectras suggests that the sample oxidized at 750 K for 5 min was either covered with an amorphous oxide, or the thickness of crystalline film was too small to produce a sufficient X-ray signal.

The major component of the reaction product formed after high temperature exposure of an AZ91D alloy was magnesium oxide MgO with a cubic structure and a lattice parameter of 4.21 Å. An example of an X-ray diffraction pattern, recorded from an oxide formed after 10 h at 710 K for 10 h, is shown in Fig. 7(c). It consists of two major peaks corresponding to 200 and 220

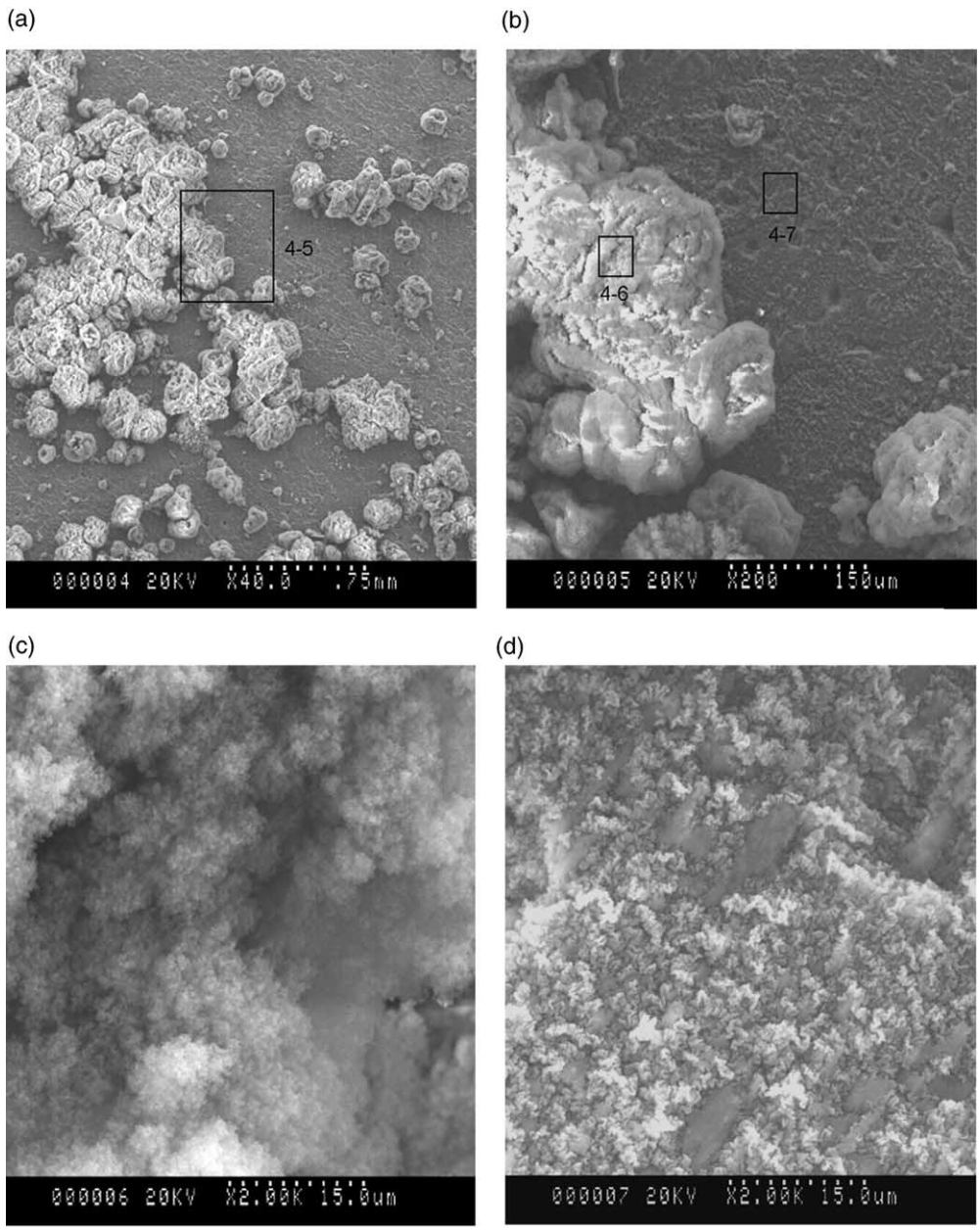

Fig. 5. SEM morphologies of the alloy surface after air exposure at 745 K for 1 h: (a) general view; (b) magnified part of an image marked as 4–5 in (a); (c) ultra-fine grain structure of the nodule marked as 4–6 in (b); (d) flat area, marked as 4–7 in (b).

crystallographic planes of MgO. An absence of Mg diffraction peaks indicates the complete oxidation within the sample volume being penetrated by X-rays and this finding coincides with macroscopic observations revealing an exclusively dark colour oxide. A colour difference as compared to gray oxide of the thin film range may be caused by a deficiency in Mg or O atoms within the MgO lat-

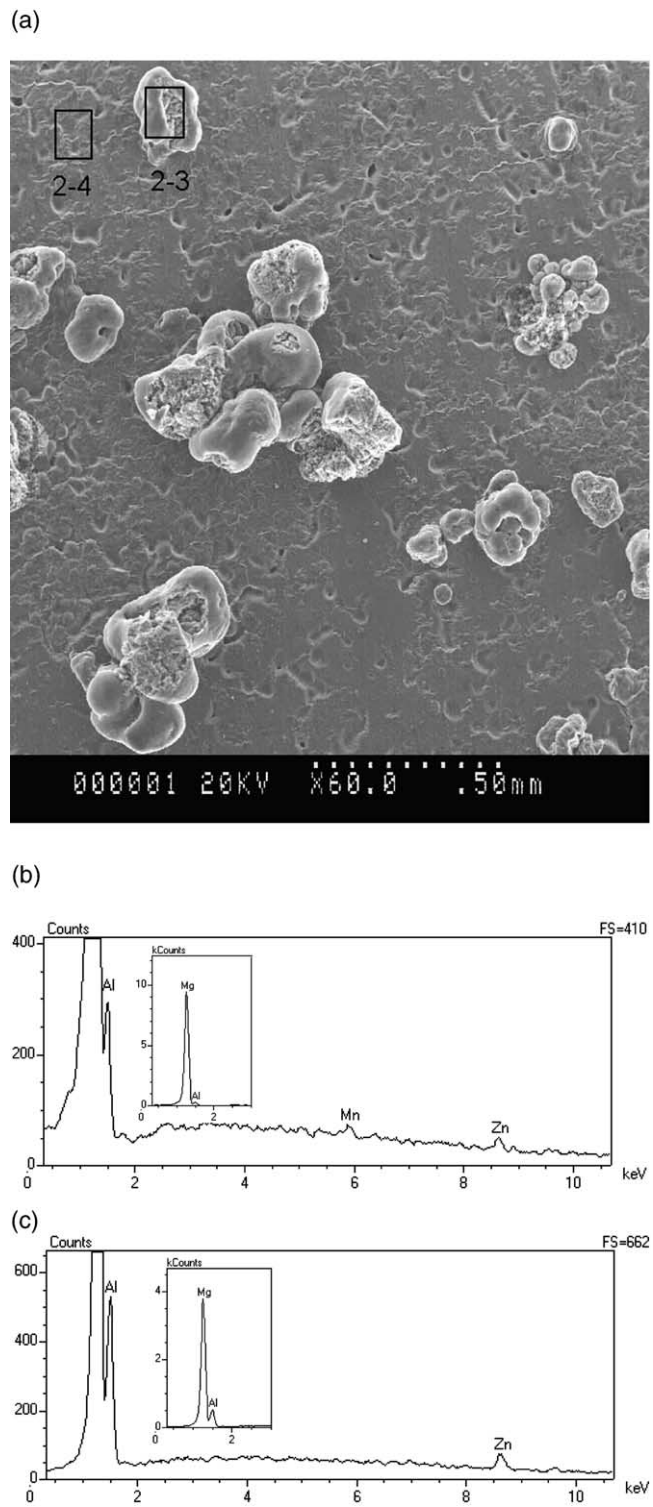

Fig. 6. SEM/EDAX analysis of the oxide formed after air exposure at 745 K for 1 h: (a) surface morphology with nodules extended from the uniform oxide; (b) EDAX spectrum from the uniform oxide marked as 2–4 in (a), the inset shows the full height of the Mg peak; (c) EDAX spectrum from the oxide nodule marked as 2–3 in (a), the inset shows the full height of the Mg peak.

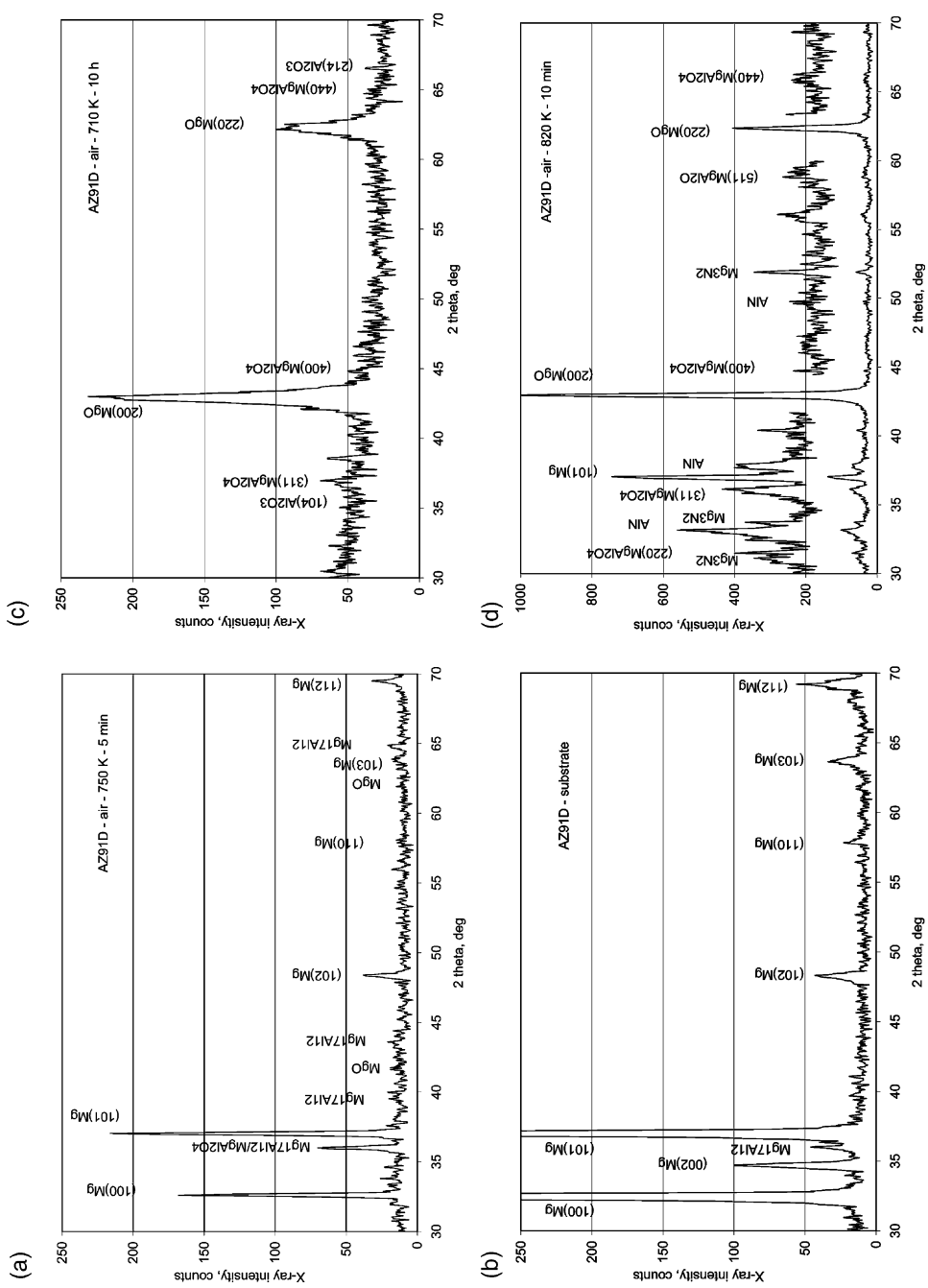

Fig. 7. X-ray diffraction patterns of oxides formed after the air exposure of AZ91D: (a) at 750 K for 5 min; (b) as in (a) after removal of the oxide film;(c) at 710 K for 10 h; (d) at 780 K for 20 min which included an ignition and combustion.

tice. Both diffraction peaks exhibit the evident broadening. Since the oxide is relatively soft and free of internal stress, it is reasonable to assume that the peak broadening was caused by an ultra fine grain. An estimation of oxide grain size was conducted using the Scherrer's [10,11] formula. Based on the corrected broadening of the 200 peak of MgO, the calculated oxide grain size equals 9.5 nm. In addition to MgO, the X-ray diffraction scan detected the presence of the magnesium aluminum oxide of $MgAl_2O_4$ spinel, having a cubic structure and a lattice parameter of 8.803 Å. The presence of Al_2O_3 alumina cannot be unambiguously proven since the suspected peaks have intensities slightly above the background noise (Fig. 7).

An essentially different diffraction pattern was recorded after reaction at 820 K. At this temperature, the initial oxidation was followed by combustion of the remaining Mg substrate (Fig. 7(d)). Due to the high temperature caused by the heat generated, the sintering and melting of the oxide formed prior to ignition took place. Although the 200 and 220 MgO peaks again dominate the diffraction scan, they have a relatively higher intensity and do not exhibit broadening. The contribution of $MgAl_2O_4$ spinel is higher than observed in Fig. 7(a). The peaks which could be associated with the presence of alumina are missing. Instead there are new peaks which indicate magnesium nitride Mg_3N_2 and aluminum nitride AlN. Their presence indicates that during combustion, nitrogen also reacted with both major constituents of the alloy. The presence of Zn was not detected in the form of a separate oxide phase.

4. Discussion of results

A high affinity of magnesium to oxygen makes it difficult to prepare oxide free surfaces during conventional open air polishing. Hence, the experiments reported here were conducted with an initial oxide film having an estimated thickness of 25 Å [12]. The film, preformed at room temperature, continued to grow firstly during heating up to the test conditions following kinetics represented by the thermogravimetric curves in Fig. 1. The maximum oxide thicknesses achieved during preheating, as converted from weight gain data, were equal to 640 and 840 Å for 470 and 760 K, respectively. This calculation is based on an assumption that at this stage the oxide is uniform in thickness and the weight gain of 1 $\mu g/cm^2$ corresponds to a 28 Å thick MgO film with a density of 3.58 g/cm^3. As pointed out in early studies by Pilling and Bedworth [13], due to the large difference in densities between the oxide and metal expressed by the MgO to Mg volume ratio of 0.81, the scale should not form a compact layer. Observations show, however, no systematic spallation of the oxide in the thin film range where it exhibits highly protective behaviour. The explanation might be the fact of the inherent strength of thin MgO film in which stress is operating in an essentially two-dimensional system and the oxide can withstand the tensile stress necessary to adapt to the dimensions of the metal. The rupturing occurs only after the film exceeds a critical thickness, as suggested previously for metallic systems [14].

The physical interpretation of the incubation period is not straightforward. The X-ray measurements did not determine the nature of initial oxides (Fig. 7(a) and (b)). A suspicion of their amorphous character does not have strong proof in the literature and "in situ" TEM observations suggest rather a crystalline structure of the initial MgO films [15]. This is in contrast to γ-Al_2O_3 protective films grown on Al–Mg alloys which tend to be amorphous at the beginning and then suffer discontinuous change of the structure [9]. It is generally accepted that the growth of compact MgO films is controlled by solid state diffusion through adherent oxide areas followed by the reaction with oxygen at the oxide/gas interface. Hence, a lack of easy-paths for fast Mg transport, as found for other crystalline oxides [16], enforcing the lattice diffusion, could be a possible explanation of highly protective behaviour. Since the diffusivity of Mg within the MgO lattice is expressed by [17]:

$$D = 1.0 \times 10^{-6}\exp(-150{,}000/RT)\ \mathrm{m^2/s} \qquad (1)$$

at 673 K the value of D is as low as 2.24×10^{-18} m^2/s justifying negligible weight gains. The outward Mg ion diffusion, leading to the inward vacancy flux, creates voids at the metal/oxide interface which not only act as channels for the transport of

Mg vapour, but also forms the local stress risers contributing to film cracking.

The top view morphology of thin oxide films does not reveal the strong correlation between the surface oxide pattern and grain boundary alignment within the underlying metal. The anisotropy is mainly expressed by thicker oxide grown in the areas covered by the intermetallic phase and it is particularly true during the transient stage between initial films and the ridges replacing them (Fig. 4(b) and (c)). In part, this supports conclusions drawn from observations of MgO growth on an Al-based alloy where oxide nucleation was not affected by the generation of slip traces, thermal grooves and grain boundaries [15]. While analyzing literature data, however, some ambiguity arises due to a lack of a precise description of surface finishing. Mechanical polishing applied here causes the deformation of a thin layer of the material which suppresses the nucleation of epitaxially oriented oxide and for some cation diffusing scales promotes the formation of randomly oriented structures over differently oriented substrate grains [18,19]. At present there is no description of how this factor affects the evolution of MgO. Crystallographically, a comparison of peak intensities on the X-ray diffraction pattern in Fig. 7(c) to that on the JCPDS standard, indicates the roughly random distribution of grain orientations within both the substrate and to the oxide, which does not allow for the determination of the crystallographic relationship between both constituents. The morphology of oxide ridges (Fig. 4(c) and (d)), which replaces initial-stage structures, is nonuniformly distributed over the alloy surface, and also does not show an obvious link with the substrate features. This type of structure indicates the formation of a fresh oxide at the oxide/metal interface, within the oxide and at the outer oxide surface. It is considered that the morphology is formed by inward oxygen transport through the cracks, followed by the reaction of oxygen with the metal at the crack walls and an outward growth of ridges [20]. The relative contribution of these processes to the overall matter transport within the scale depends on the extent of cracks and on the stage of their healing by the freshly formed oxide.

The oxidation of an alloy is affected by its phase composition and the distribution of alloying elements between phases at the reaction temperature. The microstructure of as-cast AZ91D is comprised of two phases: the α matrix, being a solid solution of Al and Zn in Mg and the precipitates of the equilibrium phase of stoichiometric composition given by $Mg_{17}Al_{12}$ (44.0 wt% Al) with an α-Mn type lattice and a cell parameter of 10.56 Å [7,21]. Under equilibrium conditions, the solubility of Al is 11.5 at.% at 710 K, but in as-cast alloys a solid solution below 710 K is enriched only with 3–4 at.% of Al. Compared with phases present in binary Mg–Al alloys, no new phases occur in ternary Mg–Al–Zn systems, if the Al to Zn ratio is greater than 3:1 and at no stage does AZ91D contain a ternary compound. It is reported that some of the Al atoms in the intermetallic compound are replaced by Zn, and at temperatures below 710 K, the intermetallics have a form of $Mg_{17}(Al,Zn)_{12}$, possibly $Mg_{17}Al_{11.5}Zn_{0.5}$ [22].

At room temperatures, there is a significant difference in corrosion resistance between AZ91D constituents. For example, in an NaCl aqueous environment the $Mg_{17}Al_{12}$ phase exhibits a better resistance by nearly one order of magnitude than α-Mg [5]. At high temperatures, especially above 710 K, the opposite behaviour is observed and $Mg_{17}Al_{12}$ experiences accelerated degradation (Fig. 7(a) and (b)). An apparent difference in the high temperature process is the fact that the chemistry and relative volumes of phases change due to diffusion. Thus, the oxidation at the gas/metal interface is superimposed on structural transformations taking place within the alloy. It is of interest that in as-cast conditions the phase composition of an AZ91D alloy deviates from the state of equilibrium (Fig. 3(a)). This implies that the heating rate to the semisolid range affects the volume, composition and also the state of the phases present. For example, the high heating rates do not allow for diffusion and cause the incipient melting of the eutectic and intermetallics. When the alloy is exposed to temperatures below that corresponding to eutectic transformation, the $Mg_{17}Al_{12}$ phase undergoes spheroidization and gradual dissolution within the Mg lattice to homogenize the alloying elements throughout the matrix (Fig. 3(b)). Of special interest for an AZ91D is Al because it is the

major alloying element and has very different oxidation and evaporation characteristics than Mg. Although Al itself forms a highly protective γ-Al_2O_3 film [20] the Al additions over 1 at.% accelerate Mg oxidation and there are proofs that for 10% Al the rate constant at 673 K increased by over two orders of magnitude [23]. To emphasize complexity, it should be mentioned that for Al-based alloys the exact opposite effect is registered and additions of Mg accelerate the oxidation process [24]. The effect of Al content within the alloy should particularly cause the oxidation difference if metal ion diffusion throughout the scale is not the rate-controlling factor but the reaction takes place at the scale/metal interface where oxygen has free access. In this case, the fact of gradual dissolution of Al should lead to an increase in the oxidation rate, as discussed above. Such expectation is not supported by this study where the oxidation rate at 660 K remains constant and no evident changes were detected at lower temperatures (Fig. 1(c)). Additions of Zn to the binary Mg–Al alloy reduce the solid solubility of Al in Mg. At high temperatures, Zn increases the Mg oxidation rate at least in part by the formation of pores within the oxide scale [23]; however, the influence of Zn is expected to be less due to its lower content.

The growth of thick MgO scales is widely considered to be controlled by linear reaction [23,25–27]. In general, this type of oxidation is insensitive to the thickness of the scale and it is assumed that oxygen can easily penetrate to the metal surface. This study revealed that for AZ91D alloy, purely linear oxidation is only valid for a certain range of temperatures and then an increase in the oxidation rate takes place (Fig. 1(b) and (c)). Further details of the interpretation of thermogravimetric kinetics were provided by microstructure observations. Firstly, an analysis revealed that an onset of non-protective oxidation is associated with the growth of oxide nodules (Fig. 1(b)and Fig. 2(b) and (c)). Secondly, the nodular growth is activated by phase inhomogeneity and in particular the formation of liquid islands of the metal and a process of Mg evaporation. Although Mg can sublimate/evaporate at a constant rate after the incubation period, by diffusion through the oxide film upon establishment of the concentration gradient, at higher temperatures rather more important is the evaporation from the metal surface if the compact oxide film breaks down to a porous layer. The specific feature of Mg is the high vapor pressure and for a vacuum environment its evaporation rate is described by the Arrhenius relation [25]:

$$K_{\text{evap}} = 0.6\exp(-25{,}000/RT)\ \text{g/cm}^2\ \text{s} \qquad (2)$$

According to a simple calculation, an evaporation of 1 μg Mg/cm^2 translates to the removal of an approximately 55.3 Å thick metal layer. The higher the reaction temperature the more evaporation beats oxidation kinetically. For the Al–Mg alloy, at 773 K the difference between evaporation and diffusion rate constants is over three orders of magnitude [25]. The microstructure shows that above 710 K, the Mg evaporation rate is so high that the vapour not only saturates all the pores within the nodule (Fig. 3(d)) but also reaches the nodule/oxygen interface where it forms a continuous film (Fig. 6(a)). It is suspected that for such a high evaporation rate, the reaction can even occur at a considerable distance from the surface and the resultant product would be released as incandescent MgO gas. Such a possibility raises some concerns on the accuracy and interpretation of TGA measurements, as discussed previously [26].

The open nodules continue to grow by the transfer of Mg vapour through voids and simultaneous reaction with oxygen, forming a product with cauliflower-like morphology. It is clear that the mechanism proposed here, and based on the saturation of scale pores by condensed metallic particles and their simultaneous reaction with oxygen, is also valid after the coalesced nodules form a continuous layer. The selective oxidation of Mg results in the formation of the alloy depleted with respect to Mg (i.e. rich in Al) as the oxide moves inward to fill the space of the consumed metal. As proven by X-ray measurements, the direct reaction between Al and oxygen occurs only during combustion (Fig. 7(d)). During gradual oxidation, Al reacts to form $MgAl_2O_4$ spinel. Although the presence of dispersed spinel particles can serve as diffusion barriers in compact scales [28], their role within loose oxide structures observed in Fig. 3(c) and (e) is certainly limited. It is postulated that a sharp acceleration of the oxidation, with an

exposure time recorded here for temperatures higher than 745 K (Fig. 1(b)), is attributed to the increased volume of voids and cracks available for the vapour condensation within thicker scales which, in turn, increases the surface area of the metal exposed to oxygen. Further increase in the oxidation rate is caused by the selective oxidation of the alloy constituents leading to a serrated interface between the oxide and metal, which increases the surface area available for evaporation.

Although precise conclusions require verification under conditions simulating the atmosphere, temperature, mechanical action and residency time of particular thermal processing, general findings of this research are of industrial importance. Assuming that a protective gas contains entrapped air causing its reactivity, at temperatures of semi-solid range the processing time is of critical importance for reducing the extent of Mg oxidation. This study shows that the incubation period preceding the onset of catastrophic oxidation favours quick processing. It is therefore reasonable to assume that the thixomolding®, with a typical residency time of semisolid Mg alloy shorter than 5 min, should result in particularly low oxygen uptake and the high integrity of the final product.

5. Conclusions

Three distinct stages were revealed during the 10 h long oxidation of an AZ91D magnesium alloy in air at temperatures between 470 and 800 K. The initial formation of the protective oxide, taking place mainly during preheating to the test temperature, is followed by an incubation period with negligible oxygen uptake. While at temperatures below approximately 610 K, the second stage lasts at least 10 h; at 710 and 760 K it is replaced within 30 and 15 min, respectively, by non-protective oxidation with a rate sharply increasing over time. At intermediate temperatures the linear reaction with a constant rate occurs between the alloy and oxygen. The eutectic melting temperature is of critical importance for an onset of non-protective oxidation and with the increased content of the liquid phase the alloy exhibits tendency to ignition and combustion.

The initial oxide grows anisotropically over the microstructural features of the substrate and has a thickness which is slightly temperature dependant. As a result of stress generation and cracking, for longer times and higher temperatures, it is transformed to oxide ridges. The growth of nodules is activated by alloy phase inhomogeneity, in particular the liquid phase in the underlying substrate. Subsequent coalescence of the nodules leads to continuous ultra-fine grained and non-protective scales with a loose structure supported by the serrated metal surface. All the oxide morphologies were comprised of magnesium oxide MgO as a dominant component, with traces of $MgAl_2O_4$ spinel. A product of alloy combustion contains additionally nitrides of Mg_3N_2 and AlN. Neither crystallographic texture within the scale, nor its epitaxy with the metallic substrate were detected.

The oxidation mechanism of an AZ91D alloy represents the complex process where structural changes within the substrate are accompanied by several surface reactions. At temperatures of solid state, the spheroidization and dissolution of intermetallics occur simultaneously with surface oxidation preferentially over the Al-rich region. At temperatures of semi-solid range, the incipient melting of the Al-rich fraction, selective evaporation of Mg from liquid islands and condensation within the scale pores and cracks are superimposed on the reaction with oxygen. An increase in the metal/oxygen interface caused by that process leads to a sharp rise in the oxidation rate.

References

[1] Avedesian MM, Baker H, editors. Magnesium and magnesium alloys. Materials Park, OH: ASM International; 1999.
[2] Baril G, Pebere N. Corros. Sci 2001;43:471.
[3] Splinter SJ, McIntyre NS, Lennard WN, Griffiths K, Palumbo G. Surface Sci 1993;292:130.
[4] Fuggle JC, Watson LM, Fabian DJ, Affrosman S. Surface Sci 1975;49:61.
[5] Song G, Atrens A, Dargusch M. Corros. Sci 1999;41:249.
[6] Mihelich J, Decker RF. Apparatus for processing corrosive molten metals. US Patent 5.711.366 (1998) and US Patent 5.819.839 (1998).
[7] Czerwinski F, Zielinska-Lipiec A, Pinet PJ, Overbeeke J. Acta Mater 2001;49:1225.

[8] Walukas DM, Decker RF, Totten AW. In: Hryn JN, editor. Magnesium technology. Warrendale, PA: TMS; 2001. p. 9-5.
[9] Tenorio JAS, Espinosa DCR. Oxidation of Metals 2000;53:361.
[10] Klug HP, Alexander LE. X-ray diffraction procedures. New York: John Wiley, 1974.
[11] Czerwinski F, Szpunar JA. J. Sol-Gel Sci. & Technol 1997;9:103.
[12] Cohen MS. Acta Metall 1960;8:356.
[13] Pilling NB, Bedworth RE. J. Inst. Metals 1923;28:534.
[14] Czerwinski F. Electrochem. Acta 1998;44:667.
[15] Scamans GM, Butler EP. Metall. Trans. A 1975;6:2054.
[16] Czerwinski F, Szpunar JA. Acta Mater 1998;46:1403.
[17] Lea C, Molinari C. J. Mater. Sci. 1984;19:2336.
[18] Czerwinski F, Smeltzer WW. J. Electrochem. Soc. 1993;140:2606.
[19] Czerwinski F. Acta Mater 2000;48:721.
[20] Jedlinski J, Bochardt G. Oxidation of Metals 1991;36:317.
[21] Roberts CS. Magnesium and its alloys. John Wiley & Sons, 1960.
[22] Aghion E, Bronfin BB. In: Lorimer GW, editor. Proceedings of the 3rd International Magnesium Conference. London: The Institute of Materials; 1997. p. 31-3.
[23] Leontis TE, Rhines FN. Trans. Amer. Inst. Mining Met. Engrs 1946;166:265.
[24] Hine RA, Guminski RD. J. Inst. Met 1960;89:417.
[25] Smeltzer WW. J. Electrochem. Soc. 1958;105:67.
[26] Gulbransen EA. Trans. Electrochem. Soc 1945;87:589.
[27] Zayan MH. Oxidation of Metals 1990;34:465.
[28] Zayan MH, Jamjoom OM, Razik NA. Oxidation of Metals 1990;34:323.